Electron mobility enhancement in AlN/GaN/AlN heterostructures with InGaN nanogrooves

E. P. Pokatilov,[a] D. L. Nika,[a] and A. A. Balandin[b]
Nano-Device Laboratory, Department of Electrical Engineering, University of California—Riverside, Riverside, California 92521

(Received 4 June 2006; accepted 17 July 2006; published online 12 September 2006)

The authors show that the electron mobility can be strongly enhanced in AlN/GaN/AlN heterostructures with the shallow $In_xGa_{1-x}N$ channel—nanogroove—in the middle of the potential well. The modified heterostructure has the room-temperature electron mobility, which is five times larger than that in conventional quantum wells. The maximum mobility enhancement is achieved for In content $x \approx 0.05$, which is sufficient to weaken the intersubband electron scattering without leading to the substantial electron—interface-phonon scattering. The mobility enhancement is pronounced for a wide range of the carrier densities ($10^{11}-10^{13}$ cm^{-2}), which is important for GaN technology. © *2006 American Institute of Physics*. [DOI: 10.1063/1.2349302]

Very recently, indium nitride (InN) attracted a lot of attention after it was discovered by Davydov *et al.*[1] and confirmed by independent studies[2,3] that its band gap is small, $E_G(\mathrm{InN})=0.7$ eV, contrary to the previously widely accepted value of nearly 2 eV. Although InN is rarely, if ever, used in devices in its binary form, when alloyed with GaN it forms a core constituent of the blue laser diode. In this letter we show that InGaN alloy utilized in electronic devices can substantially improve the room-temperature carrier mobility in wurtzite AlN/GaN/AlN heterostructures, which is limited by the polar optical phonons. Our approach for the mobility enhancement is based on the combination of the electron band-gap engineering and the phonon engineering ideas.[4] In the proposed heterostructure InN is used as an example of material, which is compatible with GaN and yet has much smaller band gap.

We consider a narrow groove made of $In_xGa_{1-x}N$ (with small In content x) inside a wurtzite AlN/GaN/AlN heterostructure, which forms a quantum well (QW). The resulting steplike profile of the confining potential is shown in Fig. 1. To demonstrate the effect we compare the electron drift mobility in the reference AlN (3 nm)/GaN (8 nm)/AlN (3 nm) QW and in QW with 2 nm wide nanogroove, i.e., AlN (3 nm)/GaN (3 nm)/$In_xGa_{1-x}N$ (2 nm)/GaN (3 nm)/AlN (3 nm). A well-known feature of wurtzite heterostructures is a strong buit-in electric field due to the induced and spontaneous polarizations.[5] The induced and spontaneous polarizations appear, correspondingly, as a result of the lattice constants mismatch at the GaN/AlN interface and the absence of inversion symmetry. The polarization is directed along c axis of a wurtzite crystal. The strength of the induced polarization depends on the AlGaN alloy composition, layer thickness, surface quality, and the growth process. The value of the built-in field can reach several MV/cm.[6]

The built-in field tilts the band diagram and creates a triangular potential well, which localizes the charge carriers. We carried our calculations for two values of the built-in field $F=600$ KV/cm and $F=1000$ KV/cm.[6] The conduction band offset at GaN/AlN interface was estimated as $E_{QW}=0.7(E_G(\mathrm{AlN})-E_G(\mathrm{GaN}))=1918$ meV. The nanogroove does not confine the electron wave function (w.f.) but affects its position in the confining AlN/GaN/AlN QW. The depth of the nanogroove is calculated as $\Delta E_0=0.8(E_G(\mathrm{GaN})-E_G(\mathrm{In_xGa_{1-x}N}))$. The band gap of $In_xGa_{1-x}N$ is approximated as $E_G(\mathrm{Ga_{1-x}In_xN})=(1-x)E_g(\mathrm{GaN})+xE_G(\mathrm{InN})-x(1-x)b$, where b is the bowing parameter and $E_G(\mathrm{InN})=0.78$ eV.[7] The reported values of the bowing parameter for InN vary from 1 to 4.5 eV, depending on the In content x.[7] We should note though that for all values of b from this interval we can obtain a nanogroove deep enough for our purposes. In the calculations, we used $b=3$ eV reported in Refs. 8 and 9 for $In_xGa_{1-x}N$ with $x<0.2$. The electron energy spectrum and w.f. have been found by solving Schrodinger equation using the standard finite-difference method.

Analysis of Fig. 1 reveals the effect of growing In concentration x in the nanogroove layer on the electron w.f. (the built-in field F is assumed to be 600 KV/cm). Due to the

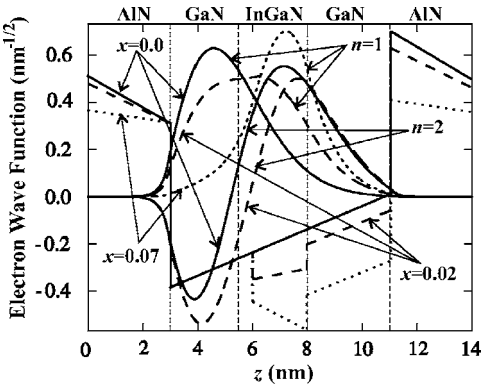

FIG. 1. Electron wave function in AlN/GaN/AlN quantum well with $In_xGa_{1-x}N$ nanogroove for several values In content x. For $x=0$ and $x=0.02$ the ground ($n=1$) and excited ($n=2$) state wave functions are shown with the solid and dashed lines, respectively. For $x=0.07$ only the ground state wave function is shown with the dotted line. The confining potentials for three values of In content x are indicated with the solid ($x=0$), dashed ($x=0.02$), and dotted ($x=0.07$) lines. The height of the confining potential at GaN/AlN interface is 1918 meV.

[a]On leave from the Department of Theoretical Physics, State University of Moldova, Kishinev, Republic of Moldova.
[b]Author to whom correspondence should be addressed; electronic mail: balandin@ee.ucr.edu

built-in field, in the conventional AlN/GaN/AlN QW the electron w.f. is squeezed to one of the AlN/GaN interfaces. In QW with $In_xGa_{1-x}N$ nanogroove, the increase in In content leads to the electron w.f. (and probability density) shift to the middle of QW, thus, among other things, reducing the electron—interface-optical-phonon interaction. For x changing from 0 to 0.02, the nanogroove depth increases but the energy difference $\Delta\varepsilon_{21}=\varepsilon_2^0-\varepsilon_1^0$ between the ground (ε_1^0) and the first excited (ε_2^0) electron states reduces (see Table I). As x continues to grow, the $\Delta\varepsilon_{21}$ trend reverses since the electron w.f. becomes more localized; the shift closer to the QW center continues. For $x=0.03$ the w.f. maximum is almost exactly in the middle of the well. The energy $\Delta\varepsilon_{21}$, the energy difference between ε_2^0, and the Fermi level E_F for different x and two values of the built-in field F are listed in Table I to elucidate the trends. The data are presented for the temperature $T=300$ K and practically relevant electron concentration $N_s=5\times10^{12}$ cm^{-2} (degenerate electron gas).

We have calculated the drift electron mobility $\mu(T)$ using the equation obtained by extending the standard formalism[10] to include the intersubband transitions

$$\mu(T)=\frac{e}{m^* k_B T}\frac{\int_0^\infty \varepsilon\tau_1(\varepsilon)f^0(\varepsilon)(1-f^0(\varepsilon))d\varepsilon+\int_0^\infty \varepsilon\tau_2(\varepsilon)f^0(\varepsilon)(1-f^0(\varepsilon))d\varepsilon}{\int_0^\infty f^0(\varepsilon_1^0+\varepsilon)d\varepsilon+\int_0^\infty f^0(\varepsilon_2^0+\varepsilon)d\varepsilon}, \tag{1}$$

where $f^0(\varepsilon)$ is the Fermi distribution, m^* is the effective mass, e is the electron charge, k_B is Boltzmann's constant, $\tau_1(\varepsilon)$ is the kinetic relaxation time of an electron with energy ε in the first (ground) subband, which includes electron transitions within the fist subband ($1\leftrightarrow1$) and transitions from the first to the second subband ($1\rightarrow2$), and $\tau_2(\varepsilon)$ is the kinetic relaxation time of an electron in the second subband, which includes transitions from the second to the first subband ($2\rightarrow1$) and the transitions within the second subband ($2\leftrightarrow2$). The kinetic relaxation times τ_1 and τ_2 have been obtained from numerical solution of the system of two integral equations, which we obtained by generalization of the Boltzmann transport equation[11] for intersubband transistions. Moreover, while solving these equations, we took into account the dispersion of optical phonons.

The reason for extra efforts on treatment of intersubband transistions is the following. For practically relevant temperature and carrier densities, the energy difference $\varepsilon_2^0-E_F$ is smaller than the optical phonon energy, which facilitates electron transitions to the excited state ε_2^0. Thus, Eq. (1) takes into account all relevant electron scattering transitions, i.e., $1\leftrightarrow1$, $1\leftrightarrow2$, and $2\leftrightarrow2$. In order to obtain accurate results for the mobility, we have evaluated matrix elements for the electron interaction with both confined (C) and interface (IF) polar optical phonons. The Hamiltonians for electron interaction with C and IF phonons have the form $\hat{H}_{\mathrm{IF,C}}=\Sigma_{\mathbf{q},\alpha}V_{\alpha;\mathrm{IF,C}}(q,z)(\hat{b}_\alpha(\mathbf{q})+\hat{b}_\alpha^\dagger(-\mathbf{q}))e^{\mathbf{iqr}}$, where $\mathbf{i}$ is the imaginary unit, $\mathbf{q}$ is the phonon vector, $\mathbf{r}$ is the two-dimensional radius vector, $\hat{b}_\alpha(\mathbf{q})(\hat{b}_\alpha^\dagger(\mathbf{q}))$ is the annihilation (creation) operator, and $V_{\alpha;\mathrm{IF,C}}(q,z)$ is the optical phonon potential for αth IF or C phonon mode, which was taken from Ref. 12. The values of the optical phonon frequencies in wurtzite GaN and AlN materials required for the calculations can be found in Ref. 13.

The phonon engineering aspect of our analysis is electron interaction with the interface phonons at the nanogroove boundaries. The $In_xGa_{1-x}N$ nanogroove has been introduce to push the electron w.f. away from the AlN/GaN interface, and tune the electron energy $\Delta\varepsilon_{21}$. From the other side, the introduction of an additional layer in the heterostructure results in additional IF phonon modes. By limiting ourselves to a certain In content range ($x\leqslant0.06$) and tuning dimensions of the heterostructure we ensure that the potentials of the interface phonon modes at the GaN/$In_xGa_{1-x}N$ boundary are negligible. The square of the ratio of IF phonon potentials $\mathbf{\Gamma}_{S,A}(z,q)=(V_{S,A;\mathrm{IF}}^{\mathrm{In_xGa_{1-x}N/GaN}}(z,q)/V_{S,A;\mathrm{IF}}^{\mathrm{GaN/AlN}}(z,q))^2$ for In content $x=0.07$ for small q and the lowest symmetric (S) and antisymmetric (A) IF modes is smaller than 0.03. As a result, the reduction of the electron mobility due to the introduction of additional $In_xGa_{1-x}N$/GaN interfaces is below 1% for $x=0.07$.

The room-temperature electron mobility μ, calculated as a function of x, is shown in Fig. 2 for three electron densities $N_s=10^{11}$ cm^{-2}, $N_s=10^{12}$ cm^{-2}, and $N_s=5\times10^{12}$ cm^{-2}. The initial mobility reduction in the interval $0<x\leqslant0.02$ is explained by the enhanced intersubband scattering due to the proximity of ε_2^0 and E_F energy levels (see Table I). Further increase of In content in the $In_xGa_{1-x}N$ nanogroove ($x\geqslant0.04$) leads to a gradual suppression of the intersubband transitions (via stronger w.f. localization), and weakens electron interaction with the AlN/GaN interface phonon modes

TABLE I. Dependence of $\Delta\varepsilon_{21}$, $\varepsilon_2^0-\varepsilon_F$, and μ on F and x.

Built-in electric field (kV/cm)	x(In)	$\Delta\varepsilon_{21}$ (meV)	$(\varepsilon_2^0-\varepsilon_F)$ (meV)	μ ($\times10^3$ cm^2/V s)
	$x=0.0$	154.9	98.8	3.54
	$x=0.02$	101.8	48.46	3.39
	$x=0.05$	181.8	123.3	16.5
$F=600$	$x=0.07$	236.5	176.9	14.5
	$x=0.0$	216.8	159.8	3.26
	$x=0.02$	117.8	63.1	3.05
	$x=0.05$	172	113.7	13
$F=1000$	$x=0.07$	228.8	169.2	12.2

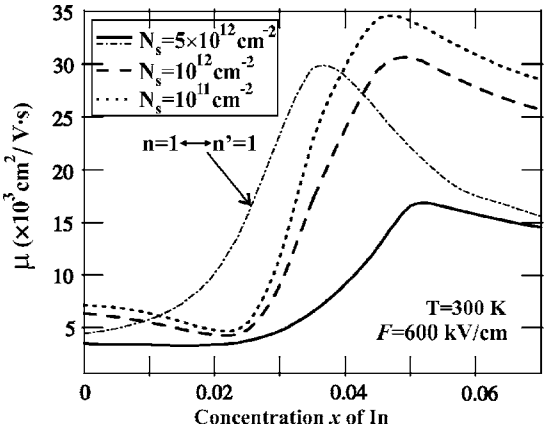

FIG. 2. Electron mobility as a function of In content x in the nanogroove. The results are shown for three electron concentrations: $N_s=5\times10^{12}$ cm^{-2} (solid), $N_s=10^{12}$ cm^{-2} (dashed), and $N_s=10^{11}$ cm^{-2} (dotted). Mobility calculated for the electron transitions within the first subband only is shown by the dash-dotted curve for $N_s=5\times10^{12}$ cm^{-2}.

owing to the w.f. shift to the QW center (see Fig. 1). At the same time, electron interaction with the confined optical phonons starts to grow due to the increase of the electron density in the middle of QW. The interplay of these trends results in a achieving a maximum mobility for x in the range of 0.045–0.055.

For $x \geqslant 0.055$, the mechanisms which led to the mobility enhancement (weakening of the intersubband transitions and suppression of the electron—interface-optical-phonon scattering) become less effective while increased localization of the electron w.f. results in growing strength of the electron interaction with confined optical phonons. The latter explains the mobility reduction for $x > 0.055$. In Fig. 2 we also show the electron mobility (dash-dotted curve), which was calculated assuming the intrasubband $(1 \leftrightarrow 1)$ scattering only, and by completely neglecting $(1 \leftrightarrow 2)$ and $(2 \leftrightarrow 2)$ scattering transitions. As one can see, this curve strongly differs from the mobility calculated with all relevant scattering mechanisms (solid curve). This confirms that in the considered heterostructures the intersubband electron transitions play an important role.

In Fig. 3 we plotted the mobility enhancement factor—ratio of the electron mobility in the AlN/GaN/AlN QW with $In_xGa_{1-x}N$ nanogroove to the electron mobility in the conventional AlN/GaN/AlN QW. The ratio, defined as $R(x,T) = \mu(x,T)/\mu(x=0,T)$, is plotted as a function of In content x and temperature T for the electron concentration of $N_e=5\times10^{12}$ cm^{-2}. The maximum enhancement $R_{\max}$ is in the range from four to five for all considered temperatures. The intriguing result is that μ enhancement is preserved at elevated $T\sim400$ K and above, which is important for GaN-based high power-density devices. Since there are no experimental data on μ in similar AlN/GaN/AlN QW, the direct comparison is not possible. Our calculated μ values are understandably higher than the measured mobility in AlGaN/GaN heterostructure field-effect transistors (HFETs).[14,15] The difference is explained by different confining potentials, built-in fields, and higher concentration of defects, and intentional and unintentional dopants in realistic GaN HFET structures. The described μ enhancement via introduction of $In_xGa_{1-x}N$ nanogroove is expected to work in the presence of the structural defects as well. The outlined approach for the mobility enhancement at room temperature and above might be useful for optimization of layout of the GaN-based high-power transistors.

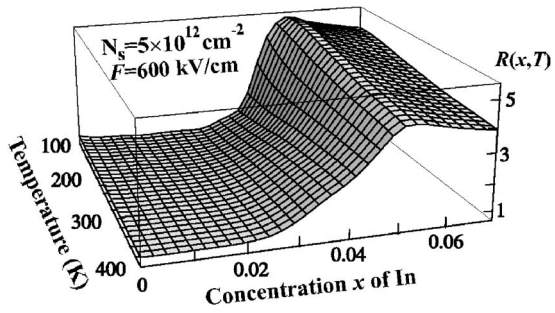

FIG. 3. Mobility enhancement factor as a function of temperature and In content x.

This work has been supported, in part, by the U.S. Civil Research and Development Foundation (CRDF) grant MOE2-3057-CS-03 to two of the authors (E.P.P.) and (A.A.B.) and by the National Science Foundation (NSF) Nanoscale Exploratory Research grant to another author (A.A.B.). One of the authors (D.L.N.) acknowledges CRDF-MRDA Young Scientist award MTFP-04-06.

[1] V. Yu. Davydov, A. A. Klochikhin, R. P. Seisyan, V. V. Emtsev, S. V. Ivanov, F. Bechstedt, J. Furthmuller, H. Harima, A. V. Mudryi, J. Aderhold, O. Semchinova, and J. Graul, Phys. Status Solidi B **229**, R1 (2002).
[2] J. Wu, W. Walukiewicz, K. M. Yu, J. W. Ager III, E. E. Haller, H. Lu, W. J. Schaff, Y. Saito, and Y. Nanishi, Appl. Phys. Lett. **80**, 3967 (2002).
[3] T. Matsuoka, H. Okamoto, M. Nakao, H. Harima, and E. Kurimoto, Appl. Phys. Lett. **81**, 1246 (2002).
[4] A. Balandin and K. L. Wang, Phys. Rev. B **58**, 1544 (1998); J. Zou and A. A. Balandin, J. Appl. Phys. **89**, 2932 (2001); E. P. Pokatilov, D. Nika, and A. A. Balandin, Appl. Phys. Lett. **85**, 825 (2004); Phys. Rev. B **72**, 113311 (2005).
[5] P. M. Asbeck, E. T. Yu, S. S. Lau, G. J. Sullivan, J. Van Hove, and J. Redwing, Electron. Lett. **33**, 1230 (1997).
[6] C. Adelmann, E. Sarigiannidou, D. Jalabert, Y. Hori, J.-L. Rouvière, B. Daudin, S. Fanget, C. Bru-Chevallier, T. Shibata, and M. Tanaka, Appl. Phys. Lett. **82**, 4154 (2003).
[7] I. Vurgaftman and J. R. Meyer, J. Appl. Phys. **94**, 3675 (2003).
[8] S. Pereira, M. R. Correia, T. Monteiro, E. Pereira, E. Alves, A. D. Sequeira, and N. Franco, Appl. Phys. Lett. **78**, 2137 (2001).
[9] F. B. Naranjo, M. A. Sánchez-García, F. Calle, E. Calleja, B. Jenichen, and K. H. Ploog, Appl. Phys. Lett. **80**, 231 (2002).
[10] J. M. Ziman, *Electrons and Phonons* (Oxford University, Oxford, UK, 1960), p. 421.
[11] N. Bannov, V. Aristov, V. Mitin, and M. A. Stroscio, Phys. Rev. B **51**, 9930 (1995).
[12] B. C. Lee, K. W. Kim, M. A. Stroscio, and M. Dutta, Phys. Rev. B **58**, 4860 (1998).
[13] P. Perlin, A. Polian, and T. Suski, Phys. Rev. B **47**, 2874 (1993).
[14] A. Balandin, S. Morozov, G. Wijeratne, S. J. Cai, R. Li, J. Li, K. L. Wang, C. R. Viswanathan, and Yu. Dubrovskii, Appl. Phys. Lett. **75**, 2064 (1999); S. L. Rumyantsev, M. E. Levinshtein, R. Gaska, M. S. Shur, A. Khan, J. W. Yang, G. Simin, A. Ping, and T. Adesida, Phys. Status Solidi A **176**, 201 (1999).
[15] V. O. Turin and A. A. Balandin, Electron. Lett. **40**, 81 (2004).